Experimental generation and dynamical reconfiguration of different circular optical lattices for applications in atom trapping

I. Ricardez-Vargas[1,2] and K. Volke-Sepúlveda[1,*]

[1]*Instituto de Física, UNAM, Apdo. Postal 20-364, 01000 México D.F., Mexico*
[2]*E-mail: ibisrv@hotmail.com*
**Corresponding author: karen@fisica.unam.mx*

Received December 16, 2009; revised March 3, 2010; accepted March 3, 2010;
posted March 4, 2010 (Doc. ID 121582); published April 20, 2010

Different configurations of optical lattices with circular cylindrical geometry have been recently studied in the context of atom trapping from a theoretical viewpoint, giving rise to a number of proposed applications. A common problem for testing theoretical predictions is the difficulty in the experimental realization of some of the necessary optical potentials. Here we discuss the experimental generation of four different circular optical lattices in an efficient and simple way using a single spatial light modulator. Our approach allows switching between different light configurations with a time resolution given by the response time of the light modulator.

OCIS codes: 260.3160, 230.6120, 020.7010, 140.3300.

1. INTRODUCTION

Nowadays, optical trapping of neutral atoms has become a common tool in many laboratories worldwide, opening the possibility of investigating new frontiers in physics. In particular, the development of far-off-resonance traps [1] has allowed the confinement and organization of cold matter in optical lattices [2]. Exciting potential applications have been envisioned for this kind of traps in several scientific and technological areas. For instance, in the realm of quantum computing, atoms trapped in optical lattices could be used to implement quantum logical gates [3].

The geometry of an optical lattice strongly determines the behavior of the trapped matter and, thus, its applications [4–6]. In this context, circular optical lattices appear as very attractive alternatives, with important differences with respect to rectangular lattices. Typically, circular lattices should be generated with light beams possessing a well defined orbital angular momentum (OAM) [7], such as Laguerre–Gaussian (LG) or Bessel beams (BBs) [8], which adds them an extra appeal since this dynamical property of the electromagnetic field can be transferred to matter. In fact, the OAM has been transferred to optically trapped microparticles [9,10], cold atom clouds [11], and—more recently—to Bose–Einstein condensates [12,13]. Another interesting property of light fields with OAM, also called optical vortices, is that they exhibit a screw type dislocation of the wave fronts associated with a rotating phase distribution [14]. It has been demonstrated that modes with phase singularities in Bose–Einstein condensates are robust to decoherence effects, opening the possibility to quantum information storage in atomic vapors [15]. In general, we will assume a harmonic time dependence of the form $\exp(-i\omega t)$, so we will look only at the spatial dependence of the wave function in each case.

Superpositions of counter-rotating optical vortices producing stationary waves in the angular direction have remarkable features as well. For instance, whereas a linear optical lattice may represent a one-dimensional quasi-periodic system only within a limited region with open boundaries, a circular lattice with a set of potential wells distributed along the angular variable is a suitable model for an unlimited one-dimensional periodic system with closed boundaries [4]. These necklace-like optical potentials have been proposed also as an interesting alternative for achieving the exchange of angular momentum between light and cold atoms [16,17]. An optical potential of this kind would split the wave function of a single localized atom into clockwise and anticlockwise components, which may interfere under certain conditions [16]. In a recent theoretical study, the interaction of a cold atom with different configurations of circular Bessel lattices was analyzed within a semi-classical approach [17]. Among other applications, the alternate operation of the different optical potentials was proposed for creating predesigned atomic paths in three dimensions [17]. Nevertheless, a practical issue that must be overcome for implementing these and other ideas experimentally is the simultaneous and efficient generation of two independently structured light beams that shall interfere to form the lattice.

The recent advances in spatial light modulation technology along with the continuous development of different algorithms to produce computer generated holograms (CGHs) have led to a great progress in the creation of structured light distributions, with especially tailored properties in intensity, in phase, or both. In fact, CGHs have been used to generate vortex beams since two decades ago [18], and these have been encoded in spatial light modulators (SLMs) for more than a decade by now [19].

In this article, we present an experimental method for the generation of four different circular optical lattices by using a phase SLM. Our code for generating the structured light beams is very simple and efficient; it consists of displaying the phase of the desired beam in the SLM. We analyze the performance of this code for the generation of multi-ringed vortex beams and necklace-like patterns by means of numerical simulations and experiments, and compare our method with previous work. In addition, we use a single SLM to independently modulate two parallel beams, which eventually interfere to form an optical lattice. The light distribution can be dynamically reconfigured by changing the hologram or phase mask displayed in the SLM.

2. OPTICAL LATTICES WITH CIRCULAR CYLINDRICAL GEOMETRY

In this study, we deal with paraxial light beams, which provide a good description for our experiments, and thus we will focus our attention on the transverse component of the optical field within a scalar approach, having a conventional polarization state. Detailed vector treatments of the wave fields studied here and other related vector light fields can be found in [17,20–25]. Under the considered conditions, a general expression for a monochromatic optical vortex on-axis, with an angular frequency ω, and propagating along the z axis can be written as

$$\Psi(\vec{r},t) = A_m(\rho,z)\exp[i(k_z z + m\varphi - \omega t)], \tag{1}$$

where k_z denotes the component of the wave vector along the propagation axis and m is an integer known as the topological charge or the order of the vortex [26]. The sign of m determines the *helicity* of the beam; this is the projection of its OAM along the propagation direction. The radius vector and the radial and angular variables are defined as usual as $\vec{r}=(x,y,z)$, $\rho=\sqrt{x^2+y^2}$, and $\tan\varphi=y/x$. The amplitude of the wave field, $A_m(\rho,z)$, is proportional to ρ^m when ρ is small.

The most typical examples of optical vortices are BBs and LG beams. In the first case, the amplitude is proportional to the Bessel function of the first type, $A_m(\rho,z)=J_m(k_t\rho)$, with k_t being the transverse component of the wave vector. BBs are propagation invariant optical fields, which means that their transverse intensity distribution does not change on propagation [8,27]. This is an idealization of course; in practice, the propagation invariance region is finite and determined by the experimental conditions. In the case of LG beams, the amplitude $A_m(\rho,z)$ is a solution of the paraxial wave equation in circular cylindrical coordinates [7,28]. In contrast with BBs, LG beams do spread on propagation, although they are structurally stable [28]. The particular propagation properties of LG modes and BBs make them suitable for different purposes; the appropriate choice depends on the specific application (see, for instance, [9,10,17,21,22,29–32]).

Linear combinations of vortex fields with exactly the same characteristic parameters but having opposite helicities yield stationary fields in the angular variable, such as

$$\Psi(\vec{r},t) = A_m(\rho,z)\begin{Bmatrix}\cos m\varphi\\ \sin m\varphi\end{Bmatrix}\exp[i(k_z z - \omega t)]. \tag{2}$$

Hereafter we will refer to these fields as angular cosine modes or simply cosine modes.

In what follows, we will briefly discuss four particular cases of circular optical lattices that can be created by means of superpositions of counter-propagating vortices or cosine modes. The first three cases were discussed in detail in [17], while the fourth case was introduced and demonstrated using sound waves in [33].

A. Three-Dimensional Stationary Circular Lattice

Consider the interference of two angular cosine modes of the type described by Eq. (2), but propagating in opposite directions along the z axis. The resulting optical field has the form

$$\Psi_{3D}(\vec{r}) = A_m(\rho,z)\cos m\varphi[\exp(ik_z z) + \exp(-ik_z z)], \tag{3}$$

with the corresponding intensity distribution

$$I_{3D}(\vec{r}) = 4A_m^2(\rho,z)\cos^2(m\varphi)\cos^2(k_z z). \tag{4}$$

There are nodal surfaces along the angular and axial coordinates. The intensity distribution for this lattice is shown in Fig. 1(a), for the case of a BB with $m=3$.

B. Toroidal Train Lattice

A set of light doughnuts arranged along an axis can be generated by the interference of two optical vortices with opposite helicities and propagating in opposite directions along the same axis. In spite of their different helicities, the two beams are rotating in the same direction with respect to a fixed reference frame [17]. The resulting field is given by

$$\Psi_{TT}(\vec{r}) = A_m(\rho,z)[\exp(ik_z z + im\varphi) + \exp(-ik_z z + im\varphi)], \tag{5}$$

leading to an intensity distribution of the form

$$I_{TT}(\vec{r}) = 4A_m^2(\rho,z)\cos^2(k_z z). \tag{6}$$

We will refer to this case as a toroidal train lattice, and it is illustrated in Fig. 1(b) for a BB with $m=1$.

C. Twisted Helical Lattice

This light configuration was first introduced by Bhattacharya for the case of LG beams [34]. A twisted helical lattice can be generated by the interference of two rotating vortices with the same helicity but counter-propagating along the same axis. This means that the two beams are rotating in opposite directions with respect to a fixed reference frame [17]. The resulting field is described by

$$\Psi_{TH}(\vec{r}) = A_m(\rho,z)[\exp\{i(k_z z + m\varphi)\} + \exp\{-i(k_z z + m\varphi)\}], \tag{7}$$

and the intensity distribution yields

$$I_{TH}(\vec{r}) = 4A_m^2(\rho,z)\cos^2(k_z z + m\varphi). \tag{8}$$

Figure 1(c) shows this optical lattice for the case of a BB with $m=2$.

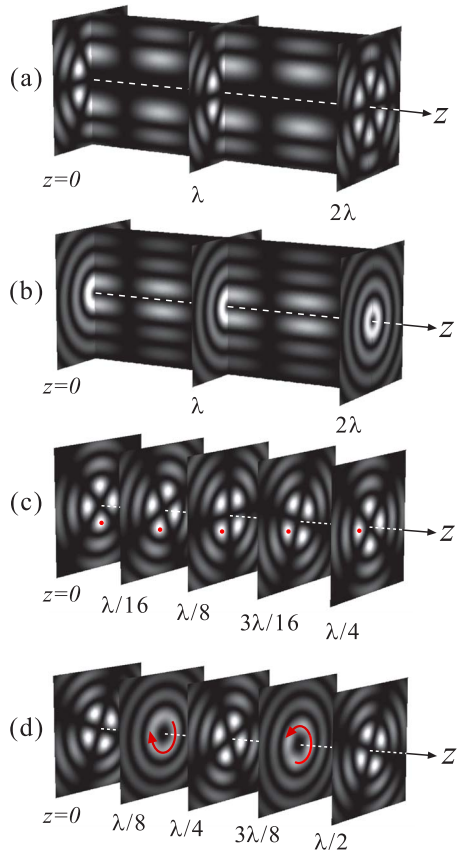

Fig. 1. (Color online) Schematic of the intensity distributions of the circular optical lattices at different planes along the propagation axis z. In all cases the radial profile corresponds to a BB. (a) Three-dimensional circular lattice, $m=3$. (b) Toroidal train lattice, $m=1$. (c) Twisted helical lattice, $m=2$; the red spot is a reference to follow the rotation of the pattern. (d) Lattice with OAM gradient, $m=2$; the red arrows indicate the rotation direction of the phase.

D. Lattice with an Orbital Angular Momentum Gradient

A peculiar optical lattice is generated by the superposition of a cosine and a sine mode propagating in opposite directions along the same axis, that is,

$$\Psi_{\mathrm{OAMG}}(\vec{r}) = A_m(\rho,z)[\sin m\varphi \exp(ik_z z) + \cos m\varphi \exp(-ik_z z)]. \quad (9)$$

The resulting intensity distribution is

$$I_{\mathrm{OAMG}}(\vec{r}) = 2A_m^2(\rho,z)(1+\sin 2l\varphi \cos(2k_z z)). \quad (10)$$

This field represents a "chain of vortices," in the sense that it is constituted by a succession of vortices along the z axis alternating opposite helicities, and between each pair of vortices, there are orthogonal cosine modes [33]. The resultant field exhibits a gradient of the OAM, which is analogous to the spin gradient or polarization gradient used for atom cooling by means of the Sisyphus effect [35]. Figure 1(d) shows the intensity distribution of this lattice for a BB with $m=2$.

We have left the radial dependence $A_m(\rho,z)$ unspecified because the most significant dynamical characteristics of the lattices studied here are associated with their angular dependence. In fact, it is worth noticing that for $m=0$, all the cases reduce to same. A standing wave of this kind, with $A_0(\rho,z)=J_0(k_t\rho)$, has been used to create a "conveyor belt" for manipulating large amounts of microparticles over extended distances [32].

3. GENERATION OF MULTI-RINGED BEAMS WITH A PHASE SLM

It is clear from the previous section that, in order to generate any of the considered optical lattices and switch among the different configurations as proposed in [17], it is necessary to independently generate the two light beams that shall interfere. This task requires a dynamical control of the light configuration, achievable by means of a SLM. In this section, we will discuss the generation of the desired optical fields by means of a phase SLM. In particular, we use a reflection spatial phase modulator (Holoeye LC-R-2500), which was characterized for a wavelength of 532 nm. The characterization process consists of determining the phase value encoded in the SLM for each gray level in the screen of the control computer [36].

One of the first techniques for producing optical vortices was the use of spiral phase plates [37], which are refractive elements whose optical width is linearly increasing along the angular variable by a complete cycle of 2π in the phase, or an integer number of cycles, for a given wavelength. Nowadays, spiral phase plates can be directly encoded with a phase SLM [38]. We follow the same idea of phase-only codification for generating both multi-ringed vortices and cosine modes [39]. Specifically, we display in the SLM the phase of a BB, either a vortex or a cosine type. We chose this multi-ringed structure of the beams because the lattices studied for atom trapping in [17], which we have closely followed, have been analyzed with BBs.

In order to analyze the optical field modulated by the SLM, we have simulated its propagation through our optical system. We consider an incident Gaussian beam of waist w_0 impinging on the SLM, in which the phase distribution of the desired beam is displayed. We use a conventional $4f$-system of spatial filtering (Fig. 2), consisting of two lenses with focal lengths f_1 and f_2. The SLM is at the back focal plane of the first lens ($z=0$); an iris diaphragm is placed at the Fourier plane ($z=2f_1$) and the modulated optical field is analyzed after the second lens ($z>2f_1+f_2$). We set $w_0=2.35$ mm, $f_1=250$ mm, and $f_2=300$ mm, in agreement with our experiment. The results

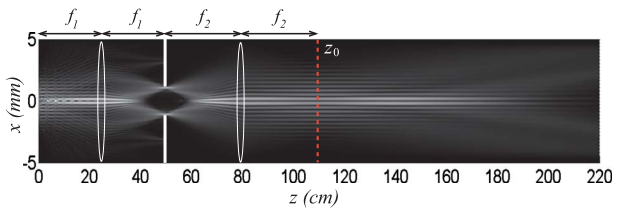

Fig. 2. (Color online) Simulation of the axial propagation of an input Gaussian beam modulated by a phase mask located at $z=0$, which encodes the phase of a Bessel vortex of topological charge $m=1$.The resulting field propagates through a lens of focal length f_1, an iris diaphragm placed at its Fourier plane ($z=2f_1$), and a second lens of focal length f_2. The plane indicated as z_0 corresponds to the back focal plane of the second lens.

of the axial propagation for a phase mask corresponding to a vortex BB of order $m=1$ and $k_t=12.8$ mm^{-1} are shown in Fig. 2. We have scaled the wavelength ($\lambda'=10\lambda$, with $\lambda=532$ nm) in order to facilitate the visualization of the spectrum details in the Fourier plane of the first lens $z=2f_1$ (the real spectrum would be ten times smaller). On the other hand, the radial profile of the Fourier spectra (FS), the transverse intensity distribution of the FS (in real units), and the generated optical fields at the focal plane of the second lens (labeled as z_0 in Fig. 2) for a multi-ringed vortex of order $m=1$ and for a cosine mode with $m=2$ are shown in the left and right columns of Fig. 3, respectively. The FS of the Bessel vortex consists of a well defined main ring in which most of the energy is concentrated and two faint rings at both sides of it (inner and outer); there are also much weaker higher diffraction orders in the form of rings with larger radii. The main ring corresponds to the spectrum of a Bessel–Gauss beam [40]; its radius $R=k_t\lambda f_1/2\pi$ is associated with the BB and its finite width $\Delta R=2\lambda f_1/w_0\pi$ is associated with the Gaussian envelope. The faint rings around the main ring give rise to additional Bessel–Gauss components of very similar transverse frequencies, which will interfere with the main beam producing intensity variations of the resulting optical field along the propagation axis (axial intensity *beatings*). A proper spatial filtering in the Fourier plane would prevent these axial intensity variations, yielding a very good approximation to a Bessel–Gauss beam; the ideal filter is a screen with an annular aperture with inner and outer radii given by $R\mp\Delta R_2$. However, a simple iris diaphragm with the right aperture ($R+\Delta R_2$) can give very reasonable results, as it is shown in the simulations in Figs. 2 and 3. The case of the cosine modes is analogous to that of the vortices.

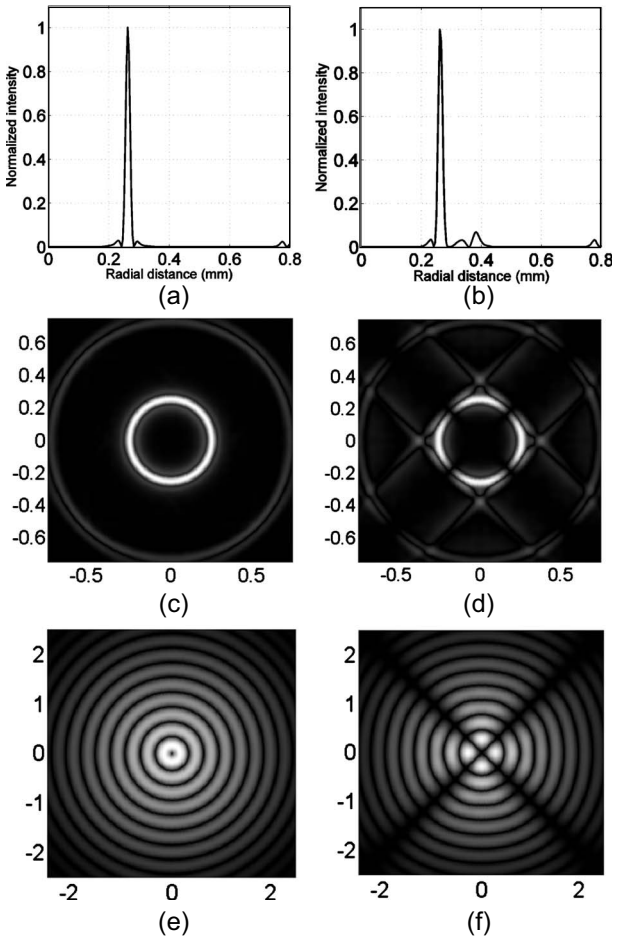

Fig. 3. Left and right columns correspond, respectively, to the case of a multi-ringed vortex of order $m=1$ and a cosine mode with $m=2$. The length scales are given in millimeters; (a) and (b) represent the radial profile of the FS; (c) and (d) show the transverse intensity distribution of the FS; (e) and (f) illustrate the generated optical fields at the plane labeled as z_0 in Fig. 2.

From our numerical calculations, we have evaluated the efficiency of the generated fields as a function of the topological charge and of the radial frequency k_t. Our findings are summarized as follows: (1) The efficiency is in general higher for the rotating modes than for the cosine modes due to a higher spreading of the Fourier spectrum in the latter case [compare Figs. 3(c) and 3(d)]. (2) The efficiency decreases as the topological charge increases; but for $m\leq 5$, the efficiency for the rotating modes is over 75%, while it is over 60% for the cosine modes. (3) The efficiency varies by less than 5% when k_t changes within the range from 6 to 14 mm^{-1}, being larger for the smaller value of k_t.

We note that a very similar method for producing vortex BBs has been recently reported [41]. In that case, the phase hologram is limited by a circular pupil and the input beam is assumed to be a plane wave. This is in contrast with the Gaussian beam illumination we consider here, which plays the role of an apodizing function, giving rise to a cleaner Fourier spectrum in the central region than that of [41] (this is what allows us to make a reasonable filtering by means of a simple iris diaphragm). In addition, it is worth to notice that the maximum propagation invariance distance of the BB generated with a phase mask is proportional to the diameter of the input beam; the smaller the beam waist of the illuminating beam, the shorter the propagation invariance distance of the generated field. In the case of a plane wave, this distance might be of several meters, and this is an advantage for alignment applications, for instance. Nevertheless, for applications requiring high energy densities, such as optical micromanipulation of particles and atom trapping, Gaussian beam illumination of the phase masks provides a better alternative since a smaller waist yields a shorter propagation invariance distance with a higher energy density.

Our numerical analysis is based on ideal conditions. However, there are unavoidable effects deteriorating the efficiency and performance of the phase masks displayed in the SLM. For instance, a common problem with SLMs is a curvature in the surface of the chip, which introduces aberrations in the modulated field. Although we obtained very reasonable results without the need for a compensation of this curvature in our masks, this effect seems to be responsible for a deterioration of the experimentally obtained field with respect to the numerical simulation, as we move away from the plane of best reconstruction (z_0). On the other hand, the partial specular reflection at the front surface of the SLM contributes with unmodulated

light traveling on-axis, which adds noise to the reconstructed field (this could be removed by using an annular filter).

4. EXPERIMENTAL SETUP

In order to generate the two independently modulated light beams required to produce any of the optical lattices with a single SLM, we have encoded what we call *dual computer generated phase masks*. Namely, we encode independent phase masks in the two halves of the modulator display. A similar approach was used before to produce vector beams [25]. The SLM should be illuminated with two parallel beams, each one of them centered with respect to the corresponding half of the SLM. In this way, a dual phase mask (DPM) can be used to modulate two beams simultaneously with a single SLM, and each DPM is associated with a particular optical lattice configuration. Our system offers the versatility to reconfigure the light distribution in one step, by switching among the different DPMs displayed in the modulator in a programmed sequence with a time resolution that is given by the response time of the specific SLM device. For example, our SLM has a typical response time of 16 ms. There are faster modulators, but the spatial resolution might be lower. Therefore, the response time of the specific SLM is a very important parameter to consider for experiments on atom trapping.

The experimental setup for the generation of circular optical lattices is shown in Fig. 4(a). A continuous wave solid state laser (Coherent Verdi V5), emitting at a 532 nm with linear output polarization state passes through a half-wave plate (HWP), and it is divided by a nonpolarizing beam splitter into two equally intense beams. Mirror M1, which diverts the transmitted beam, is mounted on a linear translation stage in order to control the separation between the parallel beams (approximately 1 cm). Both beams impinge on the SLM with a small angle and, after being modulated and reflected, pass through a linear polarizer P. The orientation of the fast axis of the HWP and the transmission axis of the polarizer P are set for optimizing the performance of the SLM [36]. After the polarizer P, a right-angle prism is introduced with the aim of increasing the separation between the beams. As discussed previously, the spatial filtering of each of the modulated beams is performed by means of two identical systems of lenses and iris diaphragms; L1-ID1-L2 and L3-ID2-L4. When the two lenses used for each spatial filtering differ in the focal length, the output beam is rescaled. In our case, the focal lengths are 25 cm for L1 and L3, and 30 cm for L2 and L4. Finally, mirrors M2 and M3 redirect the beams along the same axis but in opposite directions. An extra pair of iris diaphragms, ID3-ID4, is introduced for alignment purposes. In fact, each beam should pass through all the four diaphragms (ID1–ID4) as illustrated in the simulation in Fig. 4(b) showing the axial propagation of one of the beams through the whole optical system after the SLM. Diaphragms ID1 and ID2 are crossed by the FS of both beams traveling in opposite directions, while diaphragms ID3 and ID4 are crossed by the generated multi-ringed beams, as indicated by the arrows in the interference region in Fig. 4(a). In this context, it is important that the plane z_0 corresponds to the common focal plane of lenses L2 and L4. The measured power efficiency of each of the reconstructed fields is up to 50%.

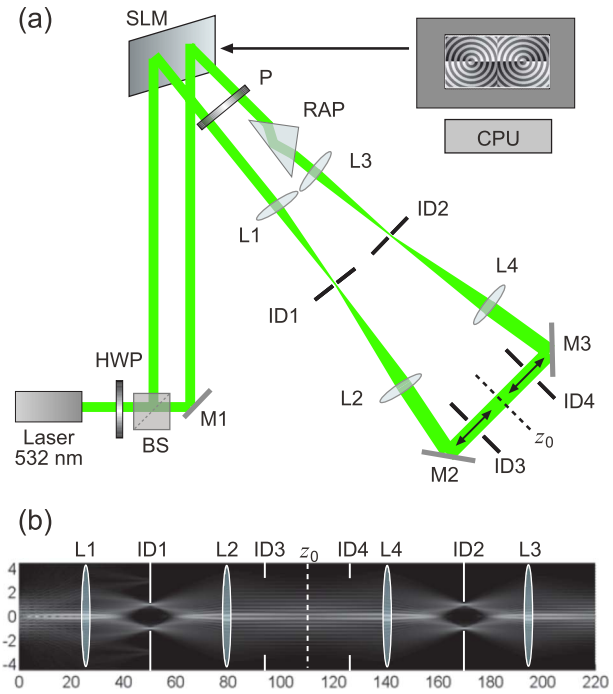

Fig. 4. (Color online) (a) Experimental setup: M1–M3, mirrors; BS, non-polarizing beam splitter; HWP, half-wave plate; SLM, spatial light modulator; P, linear polarizer; RAP, right angle prism; L1–L4, spatial filtering lenses; ID1–ID4, iris diaphragms. (b) Numerical simulation of the axial propagation of one of the beams through the whole optical system.

5. EXPERIMENTAL RESULTS AND DISCUSSION

It is well known that the first demonstration of standing waves with light was due to Wiener, who placed an inclined photographic plate in the space region occupied by the standing waves, in such a way that the period of the registered fringes depended on the inclination of the plate with respect to the common propagation axis [42]. This cannot be done for the case of structured light beams forming a standing wave since the inclination of the photographic plate would distort the transverse structure of the beams. Instead, we present all the necessary indirect evidence to infer the existence of the optical lattices in our experimental setup.

Firstly, we analyzed each of the generated light beams separately. In particular, we demonstrated that the light fields are propagation invariant over a region of several centimeters, which is in agreement with what we expected from our numerical simulations for the given waist size of the illuminating Gaussian beam. Secondly, we verified for the case of the vortices that the energy flux is spiraling on propagation, which is a signature of the rotating phase distribution [43]. Finally, the two beams have the same intensity, and the coherence and the polarization properties necessary for the interference are granted in our experimental setup in a natural way.

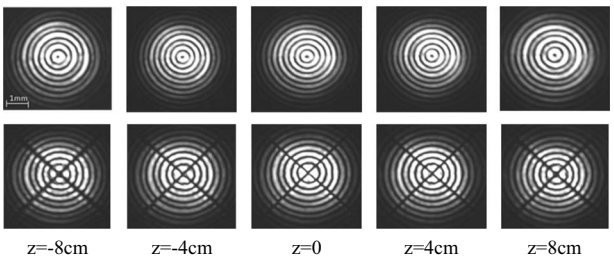

Fig. 5. Test of the propagation invariance of the generated optical fields. Top row: rotating BB with $m=1$. Bottom row: cosine BB with $m=2$. The reference plane $z=0$ corresponds to the best reconstruction.

Figure 5 shows two sets of images illustrating the propagation invariance for two examples of the different light beams that were generated. The top row corresponds to a multi-ringed vortex of order $m=1$, and the bottom row presents a cosine mode of order $m=2$. The transverse plane with the best field reconstruction is set as $z=0$ (indicated as z_0 in Figs. 2 and 4), and the distances measured at the left and right hand sides of this plane are taken as negative and positive, respectively. In the simulation in Fig. 2, this region is comprised within the axial interval $103\ \text{cm} \leq z \leq 118\ \text{cm}$.

For determining the phase behavior of the different light beams, and in particular of the vortex beams, we used two different methods: the knife edge probe [43] and direct interference with a plane wave. Figure 6 illustrates the results of the knife edge probe for a multi-ringed vortex with $m=-1$ [Fig. 6(a)], a multi-ringed vortex with $m=1$ [Fig. 6(b)], and a cosine mode with $m=3$ [Fig. 6(c)]. The left column illustrates the images of the beams when the knife edge is at the plane z_0 and the charge-coupled device camera is placed as close as possible from it (approximately 1 cm away), and the right column shows the same beams when the camera is moved at a distance $z=8$ cm away from the knife edge. It is seen from the images in the right column that the diffraction pattern spreads straight upward for the non-rotating beam (c), while it spreads asymmetrically in the case of rotating beams (a) and (b), with opposite asymmetry. This is an indicative of the rotating energy flux in the case of optical vortices, where the rotation direction is associated with the beam helicity [43]. On the other hand, Fig. 7 shows the interference of a plane wave with a multi-ringed vortex with $m=1$ propagating with a small angle relative to each other. A fork-like pattern at the beam center can be clearly identified, characteristic of the interference between a vortex and a plane wave [18]. Also, there is a π-phase shift between consecutive rings of the beam, as it can be noted from the shift of the interference fringes.

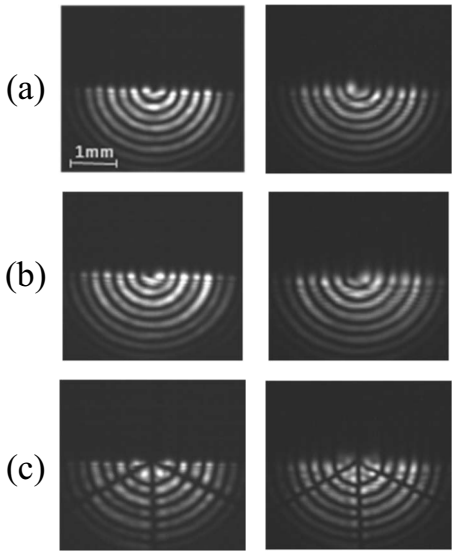

Fig. 6. Knife edge test for some of the generated light beams. The left column illustrates the images when the knife is placed at the plane $z=0$ and the camera is at the closest possible position. The right column shows the same beams when the camera is placed 8 cm away from the knife edge. Rows: (a) Multi-ringed vortex with $m=-1$. (b) Multi-ringed vortex with $m=1$. (c) Cosine mode with $m=3$.

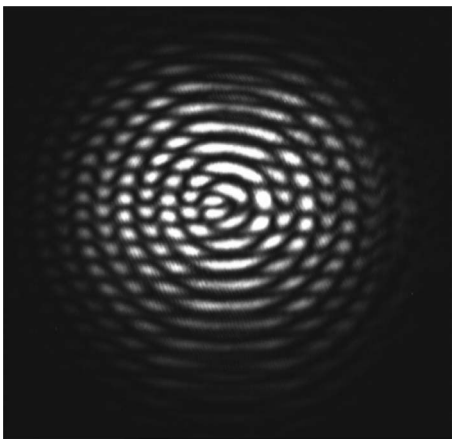

Fig. 7. Interference pattern formed by the superposition of a plane wave and a vortex BB with $m=1$, propagating with a small angle relative to each other.

Finally, having verified that the generated beams possess all the expected properties, a summary of our results for the generation of the proposed optical lattices is presented in the form of a table in Fig. 8. From left to right, the columns indicate the lattice configuration, the DPM that should be used for its generation, and the two obtained beams. From top to bottom, the topological charges of the lattices correspond to $m=3$, $m=1$, $m=2$, $m=2$.

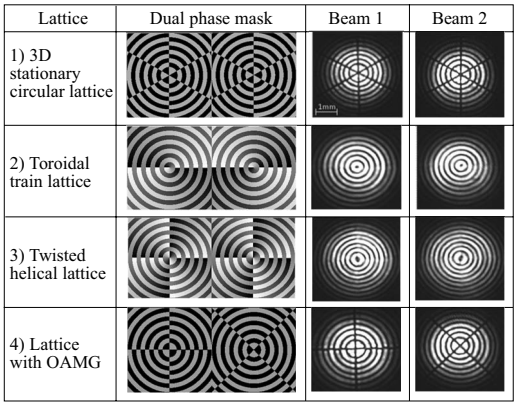

Fig. 8. Summary of the experimental results for the generation of the different optical lattices, indicating the DPM in each case, and the two generated beams.

6. CONCLUSIONS

In conclusion, we have proposed a simple and efficient experimental scheme for generating four different configurations of optical lattices with circular cylindrical geometry using a single spatial light modulator (SLM). Our scheme is based on the display of dual computer generated phase masks in the SLM, which is illuminated with two parallel light beams. Each of the parallel beams is independently modulated by the corresponding half of the dual phase mask (DPM), and then they are filtered and redirected in order to counter-propagate along the same axis to form the desired optical lattices. By changing the phase mask displayed in the SLM, it is possible to switch between different configurations of optical lattices in a single step, with a time resolution given by the response time of the SLM.

Although the periodicity of the standing waves along the common propagation axis is too small to be observed directly ($\lambda/2$), we presented all the necessary indirect evidence to prove that our experimental scheme is suitable for creating the different proposed configurations of optical lattices with circular cylindrical geometry. Namely, the two beams had the same intensity, our experimental setup naturally granted the parallel polarization states of the interfering beams, we used a laser source of extremely high coherence, and we thoroughly tested that all the generated beams had the necessary characteristics to form the lattices. Specifically, we verified that the generated light fields were propagation invariant over the necessary distance, in our case, of several centimeters. We analyzed as well the phase behavior of the different light fields by determining the energy flux direction with the knife edge test and also by means of direct interference with a plane wave. We offered in this way a simple tool for implementing different kinds of optical lattices with circular cylindrical geometry in experiments with cold atoms and Bose–Einstein condensates.

ACKNOWLEDGMENTS

We thank Dr. Victor Arrizon and M. Sc. Ulises Ruiz for their valuable help in the process of characterization of the SLM. We are grateful to Dr. Victor Arrizon and Dr. David Sánchez-de-la-Llave for useful discussions. I. Ricardez-Vargas acknowledges financial support from Consejo Nacional de Ciencia y Tecnologia (CONACYT), Mexico, for the postdoctoral position. Authors acknowledge support from Direccion General de Asuntos del Personal Academico (DGAPA-UNAM) grant PAPIIT-IN100110.

REFERENCES

1. J. D. Miller, R. A. Cline, and D. J. Heinzen, "Far-off-resonance optical trapping of atoms," Phys. Rev. A **47**, R4567–R4570 (1993).
2. P. S. Jessen and I. H. Deutsch, "Optical lattices," Adv. At., Mol., Opt. Phys. **37**, 95–139 (1996).
3. G. K. Brennen, C. M. Caves, P. S. Jessen, and I. H. Deutsch, "Quantum logic gates in optical lattices," Phys. Rev. Lett. **82**, 1060–1063 (1999).
4. L. Amico, A. Osterloh, and F. Cataliotti, "Quantum many particle systems in ring-shaped optical lattices," Phys. Rev. Lett. **95**, 063201 (2005).
5. B. M. Peden, R. Bhat, M. Kramer, and M. J. Holland, "Quasi-angular momentum of Bose and Fermi gases in rotating optical lattices," J. Phys. B **40**, 3725–3744 (2007).
6. T. Wang and S. F. Yelin, "Fast mode of rotated atoms in one-dimensional lattice rings," Phys. Rev. A **76**, 033619 (2007).
7. L. Allen, M. W. Beijersbergen, R. J. C. Spreeuw, and J. P. Woerdman, "Orbital angular momentum of light and the transformation of Laguerre–Gaussian laser modes," Phys. Rev. A **45**, 8185–8189 (1992).
8. J. Durnin, J. J. Miceli, and J. H. Eberly, "Diffraction-free beams," Phys. Rev. Lett. **58**, 1499–1501 (1987).
9. H. He, M. E. J. Friese, N. R. Heckenberg, and H. Rubinsztein-Dunlop, "Direct observation of transfer of angular momentum to absorptive particles from a laser beam with a phase singularity," Phys. Rev. Lett. **75**, 826–829 (1995).
10. K. Volke-Sepúlveda, V. Garcés-Chávez, S. Chávez-Cerda, J. Arlt, and K. Dholakia, "Orbital angular momentum of a high-order Bessel light beam," J. Opt. B: Quantum Semiclassical Opt. **4**, S82–S88 (2002).
11. J. W. R. Tabosa and D. V. Petrov, "Optical pumping of orbital angular momentum of light in cold cesium atoms," Phys. Rev. Lett. **83**, 4967–4970 (1999).
12. M. F. Andersen, C. Ryu, P. Clade, V. Natarajan, A. Vaziri, K. Helmerson, and W. D. Phillips, "Quantized rotation of atoms from photons with orbital angular momentum," Phys. Rev. Lett. **97**, 170406 (2006).
13. C. Ryu, M. F. Andersen, P. Clade, V. Natarajan, K. Helmerson, and W. D. Phillips, "Observation of persistent flow of a Bose–Einstein condensate in a toroidal trap," Phys. Rev. Lett. **99**, 260401 (2007).
14. J. F. Nye and M. V. Berry, "Dislocations in wave trains," Proc. R. Soc. London, Ser. A **336**, 165–190 (1974).
15. R. Pugatch, M. Shuker, O. Firstenberg, A. Ron, and N. Davidson, "Topological stability of stored optical vortices," Phys. Rev. Lett. **98**, 203601 (2007).
16. H. L. Haroutyunyan and G. Nienhuis, "Diffraction by circular optical lattices," Phys. Rev. A **70**, 063408 (2004).
17. K. Volke-Sepúlveda and R. Jáuregui, "All-optical 3D atomic loops generated with Bessel light fields," J. Phys. B **42**, 085303 (2009).
18. A. Vasara, J. Turunen, and A. Friberg, "Realization of general nondiffracting beams with computer-generated holograms," J. Opt. Soc. Am. A **6**, 1748–1754 (1989).
19. J. A. Davis, J. Guertin, and D. M. Cottrell, "Diffraction-free beams generated with programmable spatial light modulators," Appl. Opt. **32**, 6368–6370 (1993).
20. Z. Bouchal and M. Olivik, "Non-diffractive vector Bessel beams," J. Mod. Opt. **42**, 1555–1566 (1995).
21. R. Jáuregui, "Rotational effects of twisted light on atoms beyond the paraxial approximation," Phys. Rev. A **70**, 033415 (2004).
22. R. Jáuregui and S. Hacyan, "Quantum-mechanical properties of Bessel beams," Phys. Rev. A **71**, 033411 (2005).
23. K. Volke-Sepúlveda and E. Ley-Koo, "General construction and connections of vector propagation invariant optical fields: TE and TM modes and polarization states," J. Opt. A, Pure Appl. Opt. **8**, 867–877 (2006).
24. A. Flores-Pérez, J. Hernández-Hernández, R. Jáuregui, and K. Volke-Sepúlveda, "Experimental generation and analysis of first-order TE and TM Bessel modes in free space," Opt. Lett. **31**, 1732–1734 (2006).
25. C. Maurer, A. Jesacher, S. Fürhapter, S. Bernet, and M. Ritsch-Marte, "Tailoring of arbitrary optical vector beams," New J. Phys. **9**, 78 (2007).
26. G. Indebetouw, "Optical vortices and their propagation," J. Mod. Opt. **40**, 73–87 (1993).
27. J. Turunen and A. T. Friberg, "Self-imaging and propagation-invariance in electromagnetic fields," Pure Appl. Opt. **2**, 51–60 (1993).
28. A. Siegman, *Lasers* (University Science Books, 1986), pp. 626–652.
29. D. McGloin and K. Dholakia, "Bessel beams: diffraction in a new light," Contemp. Phys. **46**, 15–28 (2005).
30. K. T. Gahagan and G. A. Swartzlander, Jr., "Trapping of

low-index microparticles in an optical vortex," J. Opt. Soc. Am. B **15**, 524–534 (1998).
31. V. Garcés-Chávez, K. Volke-Sepúlveda, S. Chávez-Cerda, W. Sibbett, and K. Dholakia, "Orbital angular momentum transfer to an optically trapped low-index particle," Phys. Rev. A **66**, 063402 (2002).
32. T. Cizmar, V. Garcés-Chávez, K. Dholakia, and P. Zemanek, "Optical conveyor belt for delivery of submicron objects," Appl. Phys. Lett. **86**, 174101 (2005).
33. A. O. Santillán, K. Volke-Sepúlveda, and A. Flores-Pérez, "Wave fields with a periodic orbital angular momentum gradient along a single axis: a chain of vortices," New J. Phys. **11**, 043004 (2009).
34. M. Bhattacharya, "Lattice with a twist: helical waveguides for ultracold matter," Opt. Commun. **279**, 219–222 (2007).
35. J. Dalibard and C. Cohen-Tannoudji, "Laser cooling below the Doppler limit by polarization gradients: simple theoretical models," J. Opt. Soc. Am. B **6**, 2023–2045 (1989).
36. U. Ruiz-Corona and V. Arrizon-Peña, "Characterization of twisted liquid crystal spatial light modulators," Proc. SPIE **6422**, 1–7 (2007).
37. M. W. Beijersbergen, R. P. C. Coerwinkel, M. Kristensen, and J. P. Woerdman, "Helical-wavefront laser beams produced with spiral phaseplate," Opt. Commun. **112**, 321–327 (1994).
38. D. Ganic, X. Gan, and M. Gu, "Optical trapping force with annular and doughnut laser beams based on vectorial diffraction," Opt. Express **13**, 1260–1265 (2005).
39. J. A. Davis, E. Carcole, and Don M. Cottrell, "Nondiffracting interference patterns generated with programmable spatial light modulators," Appl. Opt. **35**, 599–602 (1996).
40. F. Gori, G. Guattari, and C. Padovani, "Bessel–Gauss beams," Opt. Commun. **64**, 491–495 (1987).
41. V. Arrizón, D. Sánchez-de-la-Llave, U. Ruiz, and G. Méndez, "Efficient generation of an arbitrary nondiffracting Bessel beam employing its phase modulation," Opt. Lett. **34**, 1456–1458 (2009).
42. M. Born and E. Wolf, *Principles of Optics*, 7th ed. (Cambridge U. Press, 1999), pp. 311–312.
43. J. Arlt, "Handedness and azimuthal energy flow of optical vortex beams," J. Mod. Opt. **50**, 1573–1580 (2003).